SOLUTION STRENGTHENING AND AGE HARDENING CAPABILITY OF Al-Mg-Mn ALLOYS WITH SMALL ADDITIONS OF Cu

Z. Zhu, M.J. Starink

Materials Research Group, School of Engineering Sciences, University of Southampton, Southampton S017 1BJ, UK

Abstract

Nine Al-(1-3)Mg-(0-0.4)Cu-0.15Si-0.25Mn (in wt%) alloys with potential applications in both packaging and automotive industries have been investigated. Tensile testing showed that solution strengthening is in good approximation linearly proportional to the Mg content. Mechanical testing and microstructural examinations of aged samples indicate that Mg_2Si phase precipitates contribute to age hardening of Cu-free alloys, whilst both Mg_2Si phase and S (Al_2CuMg) phases contribute to that of Cu-containing alloys. The age hardening capability is critically influenced by solution treatment temperature: increasing the solution treatment temperature from 500 to 550°C results in a marked increase in rate of hardening for Cu containing alloys and solution treatment at about 550°C or higher is needed to allow Mg_2Si phase precipitation during ageing in Cu-free alloys with Mg content of about 2% or higher.

1. Introduction

Aluminium alloys are used in a wide range of applications in transport, packaging, building and general engineering sectors. The alloys studied in this work, with compositions in the range Al-(1-3)wt%Mg-0.2wt%Mn-0.2wt%Fe-0.2wt%Si-(0-0.4)wt%Cu, encompass alloy compositions that are employed in canstock and compositions that have potential for application in cars. Al-Mn based (3XXX) and Al-Mg based (5XXX) alloys have been widely used in beverage cans for decades [1,2,3,4]. Specifically, AA3104/3004 (compositions typically around Al-1Mg-1Mn-0.2Cu-(0.3-0.6)Si-0.5Fe) and AA5182 (composition around Al-4Mg-0.3Mn-0.1Cu-0.2Si-0.2Fe) alloys have long been used as can body stock and can end stock, respectively. Although the market now is mature, there is a fierce competition coming from alternative materials such as steel, polyethylene tetraphthalate (PET) etc. [1,2]. The solution to improving the competitiveness of Al alloys is to reduce the costs by improving process efficiency and innovations in weight reduction or downgauging of the canstock [1,2,4]. Therefore, it is essential to understand (both qualitatively and quantitatively) the relation between processing, microstructure and properties.

In recent decades, there is a trend in the automobile industry to use aluminium alloys as car body panels to reduce weight and thus improve fuel economy and emissions [5]. Both 5XXX Al-Mg alloys, which are mostly non-heat-treatable, and heat-treatable Al-Cu, Al-Mg-Si-Cu and Al-Mg-Si alloys of 2XXX and 6XXX series are used. Although the Al-Mg-Mn 5XXX alloys have good formability, they have a relatively low strength with a tendency of Lüders band formation [6,7], which restricts their use to interior structural applications [5]. Hence, for automotive applications, there is a growing trend to exploit new alloys [8,9]. 5XXX alloys (especially AA5182 and AA5052 (composition around Al-3Mg-0.3Mn-0.1Cu-0.2Si)) with small Cu additions are very promising candidates for these applications because of their excellent formability, good strength and the

benefits of precipitation hardening during paint-baking due to Cu additions [10]. However, precipitation hardening induced by Cu additions may make the interactions between work hardening, recovery and precipitation more complicated during processing.

Canstock sheet production involves a number of thermomechanical processing steps, starting with DC ingot casting followed by homogenisation, hot rolling, annealing and cold rolling. Homogenisation usually occurs at two temperatures, e.g. starting at about 570°C followed by slow cooling to about 510°C. Its main objectives in the can making process are the elimination of microsegregation, the transformation of the Al_6(Fe,Mn) coarse particles to α-Al_{12}(Fe,Mn)$_3$Si particles [11] and the redistribution of Mn from solid solution to coarse particles and dispersoids. During the relatively slow commercial heat up of an ingot, a uniform distribution of Mg, Cu and Si can be achieved after heating up to 500°C [12]. A range of further hot and cold rolling steps follow, and can bodies are produced by a draw & iron (D&I) process. The can body needs to be able to withstand a minimum dome reversal pressure, and have vertical load bearing capacity, making strength an important consideration too. Higher strength enables thinner sheet to be used and hence a more efficient use of material in the fabrication of the product. Surface qualities of the sheet are also important, both in terms of surface finish for the product and for good frictional characteristics between the sheet surface and the forming dies.

The alloys used for the above-mentioned canstock and automotive applications are generally based on Al-Mg-Mn alloys with small additions of Cu. The alloys are warm or cold rolled to achieve thin gauge. During the processing of alloys with Cu additions, precipitation of strengthening phases occurs during hot and cold rolling as well as during heat treatment after cold rolling [13]. In both cases, precipitation will change the yield stress and the work hardening, which will affect subsequent further working of the alloys. After cold rolling, the alloys for beverage can application are used in a work hardened condition, but for the car body application, they will be supplied to car manufacturers with O temper (annealed) due to the higher requirement of excellent formability during car body forming. For both applications, coating/painting and baking are needed as a final procedure. Both recovery and precipitation will occur during the baking process of the cold worked alloys.

The present paper reports work on nine alloys in the range Al-(1-3)wt%Mg-0.2wt%Mn-0.2wt%Fe-0.2wt%Si-(0-0.4)wt%Cu. These low Cu additions are effectively microalloying additions, causing changes in the amount of secondary phases that are very small compared with the amounts present without the Cu additions [14]. As part of a larger study into modelling of microstructure evolution and mechanical properties, we here present an analysis of the solution strengthening and age hardening capability of the alloys after solution treatment.

2   Experimental

In this study, nine Al-(1-3)Mg-(0-0.4)Cu-Mn-Fe-Si alloys (in wt%) were investigated. The alloys were produced at the former Alcan Banbury Labs, Banbury, UK, and their compositions are shown in Table I. All alloys were direct chill (DC) cast. The cast ingots were preheated and homogenised at 540°C, and subsequently hot rolled down to 5mm in thickness. After that, the hot rolled sheets were solution treated at 500°C for 20 minutes, followed by cold rolling to 10% and 40% reduction. Transmission electron microscopy and electron backscatter diffraction studies of the as cold-rolled

material were reported elsewhere [15]. Specimens of 40% cold rolled alloys were re-solution treated at 500°C/30min and 550°C/30min for mechanical testing and age hardening experiments.

The tensile testing specimens were designed based on and within the specification of the ASTM-E8M standard. To provide a valid measurement of sample elongation and elongation to failure, samples should fail in a smooth section between the points of attachment of the extensometer. To ensure this, a small modification of the design of tensile specimens was adopted which entailed a small and gradual change in the cross sectional area of about 0.8% such that the minimum cross sectional area is located in the middle of the gauge length of the sample. Therefore, a specimen with this geometry is prone to fracture at the middle of the gauge length during tensile testing due to the highest stress occurring in this section. The tensile axis is taken in the longitudinal (L) direction (i.e. the rolling direction). Tensile testing was performed on the freshly solution treated samples solutionised at 500°C to evaluate solution strengthening due to Mg and Cu. Tensile tests were performed using an 8800 series Instron machine at a constant strain rate of 0.001 s^{-1}. For each condition usually two tests were performed. The difference in elongation to failure between two tests is on average 3%; i.e. the confidence in the reported average is about 1.5%. The difference in 0.2% proof strength between two tests is on average 3MPa, i.e. the confidence in the reported average is about 1.5MPa.

For age-hardening tests, solution treated samples were isothermally aged at 170°C in an oven. Hardness tests were performed using a micro-Vickers hardness tester with 1 kg load held for 15s. The mean of 5 indentations was taken as the hardness of the corresponding condition.

Table I Compositions of the alloys studied (in wt%)

Alloy No.	Mg	Cu	Mn	Fe	Si	Al
A1	1.02	<.01	0.25	0.22	0.16	
A2	1.96	<.01	0.25	0.20	0.15	
A3	2.95	<.01	0.24	0.20	0.15	
A4	1.01	0.18	0.26	0.21	0.14	
A5	1.91	0.18	0.25	0.19	0.14	bal.
A6	2.99	0.19	0.24	0.19	0.15	
A7	1.03	0.39	0.26	0.20	0.14	
A8	1.98	0.39	0.25	0.21	0.15	
A9	2.9	0.4	0.25	0.19	0.15	

For analyses by differential scanning calorimetry (DSC), small disks were prepared. The DSC experiments were conducted in a Perkin-Elmer Pyris 1 DSC. All experiments were run at a constant heating rate of 10°C/min. Details and methodology for DSC experiments and baseline correction are provided elsewhere [16]. In the present alloys, the heat effects are very small, and hence baseline correction proved challenging. In the presented DSC thermograms, baseline correction using a linear function was conducted, and remaining uncertainties on position of baseline are in the order of 2mW/g in the range up to 400°C.

Samples for analysis by a field emission gun scanning electron microscope (FEG-SEM) were cut from cold rolled sheets with 10% reduction and then cold mounted. Subsequently, they were ground and polished using standard procedures. FEG-SEM observations were conducted on a JSM-6500

scanning electron microscope for intermetallics analysis. The FEG-SEM was equipped with an energy dispersive spectrometer (EDS) for compositional analysis.

3 Results and discussion

3.1 Intermetallic particles

Intermetallic analysis by SEM/EDS was performed on the cold worked samples of alloys A1, A2, A3, A4, A5 and A9. Cold-rolled alloy A9 was selected for detailed intermetallics analyses, and example of particles observed by SEM is presented in Fig. 1. The particles are generally aligned in the rolling direction. For one group of particles, which appear bright in the backscatterred electron imaging (BEI) mode, the EDS results reveal the presence of Cu, Fe, Mn and Si. A plot of Si:(Fe+Mn+Cu) ratio vs. Al:(Fe+Mn+Cu) ratio (Fig. 2) shows that these particles can be classified into two groups. Thermodynamic simulations (see below) and various microstructural studies on similar alloys (see e.g. [11,17]) have indicated that these alloys contain two Mn and Fe containing phases: $Al_6(Fe,Mn,Cu)$ and $Al_{12}(Fe,Mn,Cu)_3Si$ (also known as the cubic alpha phase). In Group I, the Si:(Fe+Mn+Cu) ratio is about 0 and the Al:(Fe+Mn+Cu) ratio is about 5~7.5. The particles in this group are identified as $Al_6(Fe,Mn,Cu)$. Most of the brighter particles are located in this group. In the other group (Group II), the Si:(Fe+Mn+Cu) ratio is about 0.25~0.3 whilst the Al:(Fe+Mn+Cu) ratio is about 7~8. The particles in group II therefore are identified as $Al_{12}(Fe,Mn,Cu)_3Si$. The Al:(Fe+Mn+Cu) ratio obtained from EDS analysis is slightly higher than that in the stoichiometry of $Al_{12}(Fe,Mn,Cu)_3Si$, which is 4. This may be due to the interactions of the surrounding Al matrix and the particles analysed. A third type of particles found in alloy A9 appears darker in the BEI images. The EDS analysis in the SEM shows it contains Mg and Si elements, with no significant amounts of other alloying elements being detected, and it may be identified as Mg_2Si phase. The observations on the presence of these particles are summarised in Table 2.

Table 2 Thermodynamic equilibrium prediction of particle content at 500°C and 540°C, and particles detected in SEM/EDS experiments (+: detected, -:not detected, blank: alloy not studied by SEM).

Alloys	$Al_{12}(Fe,Mn)_3Si$			Mg_2Si		
	540°C	500°C	exp.	540°C	500°C	exp.
A1	0.86	1.349	+	0	0	-
A2	0.78	0	+	0	0.295	+
A3	0	0	+	0.268	0.357	+
A4	0.67	1.167	+	0	0	-
A5	0.73	0	+	0	0.263	+
A6	0	0		0.271	0.358	
A7	0.780	1.238		0	0	
A9	0	0	+	0.263	0.355	+

It should also be noted that the occurrence of variable amounts of oxygen in the EDS spectrum for Mg_2Si phase was noted. It has been mentioned in the literature that Mg_2Si phase decomposes in water [18], and it was found that Mg_2Si particles might begin to dissolve during water polishing

[19]. The reason why it decomposes or dissolves in water may be explained by the following reaction [20]:

$$Mg_2Si + 4H_2O \rightarrow SiH_4(g) + 2Mg(OH)_2$$

And the following reactions may further occur under certain conditions:

$$Mg(OH)_2 \rightarrow MgO + H_2O$$
$$SiH_4 + 2O_2 \rightarrow SiO_2 + 2H_2O$$
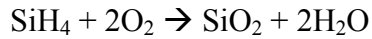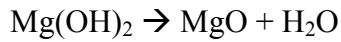
Therefore, Mg_2Si may be dissolved during water polishing. (To avoid the decomposition of Mg_2Si during polishing, alcohol instead of water may be used, but this was not applied in the present work.)

Prediction of phase diagram can be achieved through computational thermodynamics based on calculating the free energy of co-existing phases present in a system by minimising the Gibbs free energy. In this study, some thermodynamic predictions made by MTDATA software will be used. From the results of the thermodynamic calculations, three types of intermetallics may form during solution treatment depending on alloy composition: $Al_6(Fe,Mn)$, $Al_{12}(Fe,Mn)_3Si$ and Mg_2Si. $Al_6(Fe,Mn)$ is predicted to be present in all the alloys at the solutionising temperatures 500°C and 540°C and the predicted amounts of $Al_{12}(Fe,Mn)_3Si$ and Mg_2Si are listed in Table 2, together with the results of experimental observations of these two phases.

The thermodynamic model predictions and SEM/EDS experimental results are in many aspects consistent with each other except for that thermodynamic model predicts that at 500°C cubic alpha particles are present only in the alloys with 1wt% Mg, and for alloys with higher Mg content, no such particles are predicted. However, cubic alpha phase was detected in all the alloys studied.
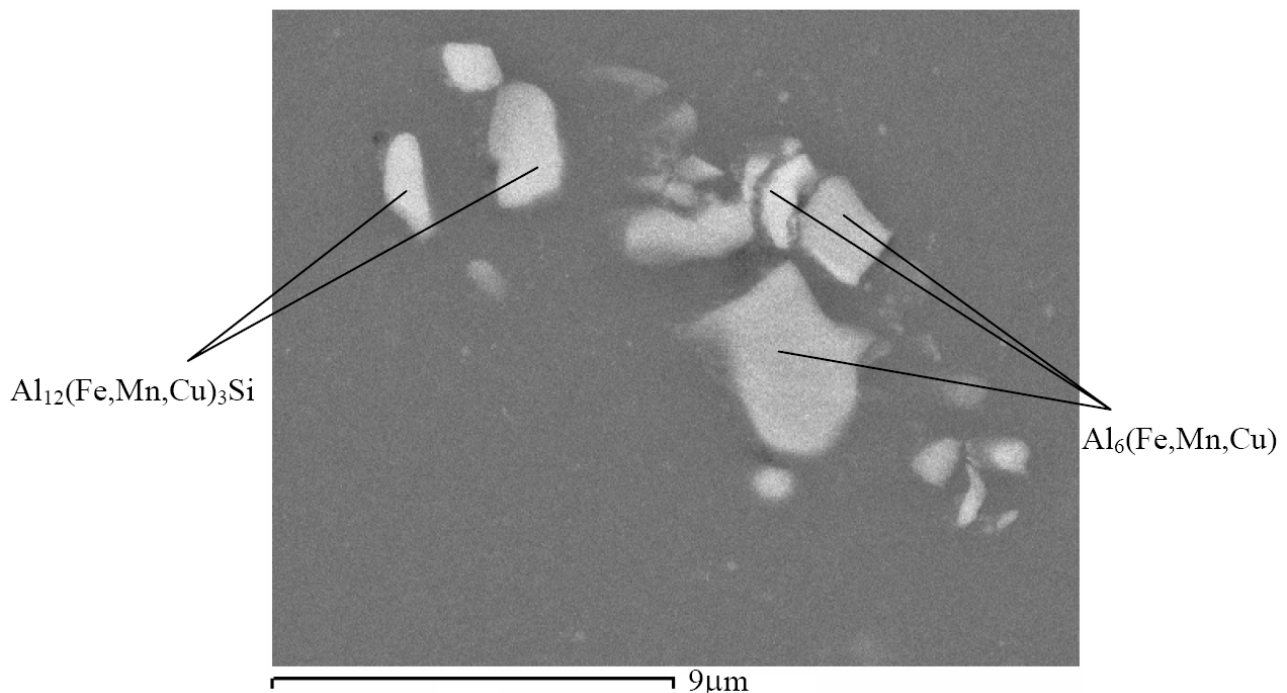

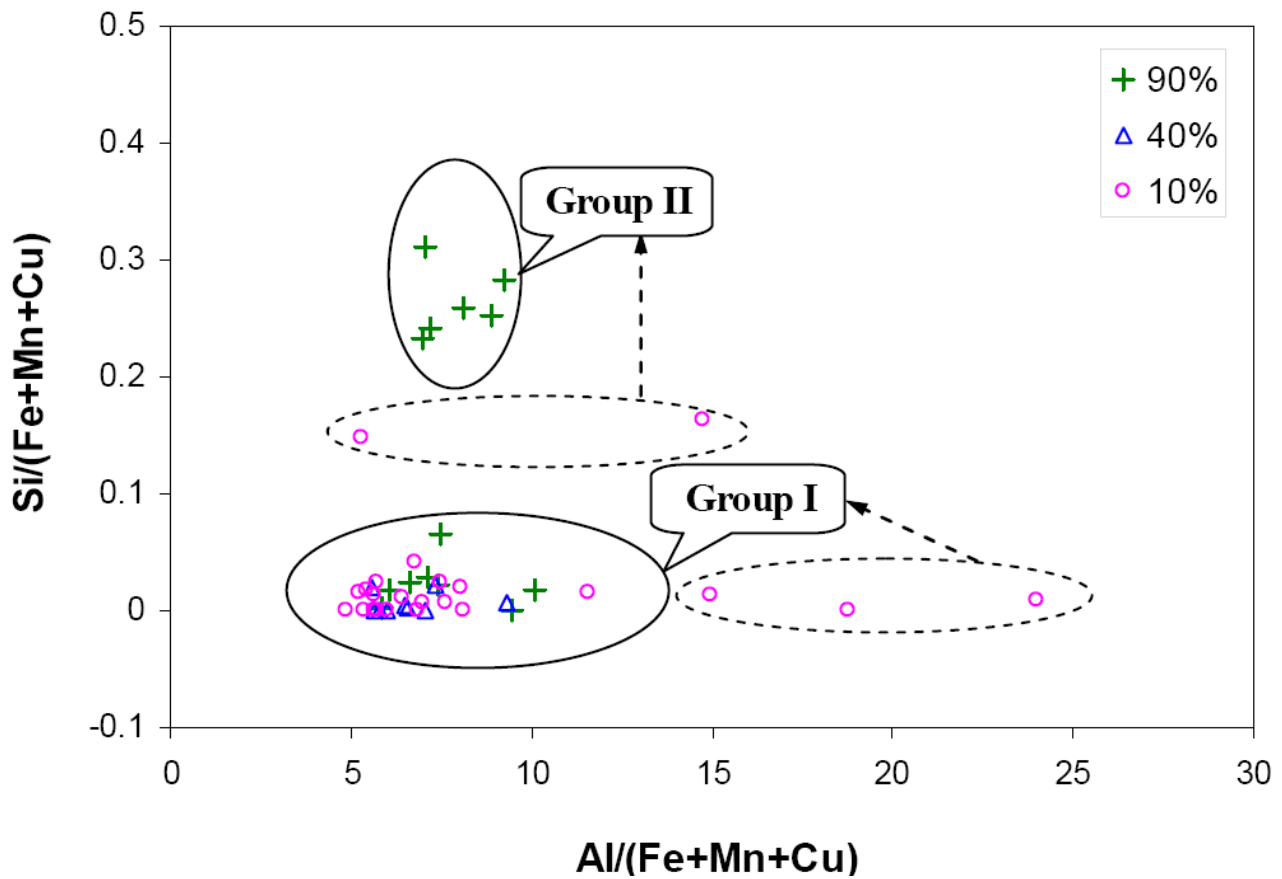Fig. 1   SEM micrograph of the bright particles identified in the cold-rolled alloy A9 (BEI mode).

Fig. 2 The Si:(Fe+Mn+Cu) ratio vs. the Al:(Fe+Mn+Cu) ratio for the bright particles in alloy A9 in 3 conditions. + : 10% cold-worked, Δ : 40% cold-worked and o : 90% cold-worked. Compositions fall into two groups (see text).

3.2   Strength of solution treated alloys

The results of tensile tests of the alloys in solution treated condition (solution treatment temperature 500ºC) are presented in Fig. 3 and Fig. 4. The results show that increasing the Mg content by 1wt% has a strong influence on the yield strength, with increasing Cu content by 0.2wt% causing a limited but detectable increase in the yield strength. Fig. 5 shows that, in common with many alloy systems, the elongation to failure tends to decrease with increasing yield strength. Cu addition appears to slightly increase the ductility at equivalent yield strength.

In order to model the yield strength of these alloys in worked and subsequently aged conditions, the following contributions have to be considered:
- Solid-solution strengthening, which is here mainly due to Mg
- Dislocation strengthening, i.e. work hardening & recovery
- Precipitation hardening
- Grain boundary strengthening
- Base strength

In the case of multicomponent alloys, a number of models [21,22,23,24,25,26,27] have been proposed to determine the strengthening effect due to dissolved alloying elements. A general form

for the increment in the critical resolved shear stress (CRSS) due to solution strengthening, $\Delta\tau_{ss}$, on the solute concentration is:

$$\Delta\tau_{ss} = \sum k_j c_j^{n_{ss}} \qquad (1)$$

where k is a constant related to the properties of the related solute j, c is the solute concentration. Theoretical treatments indicate n could equal 2/3, 1 or 1/2 [24]. The yield strength of solution treated alloys, that have negligible strengthening contributions due to dislocations, is written as:

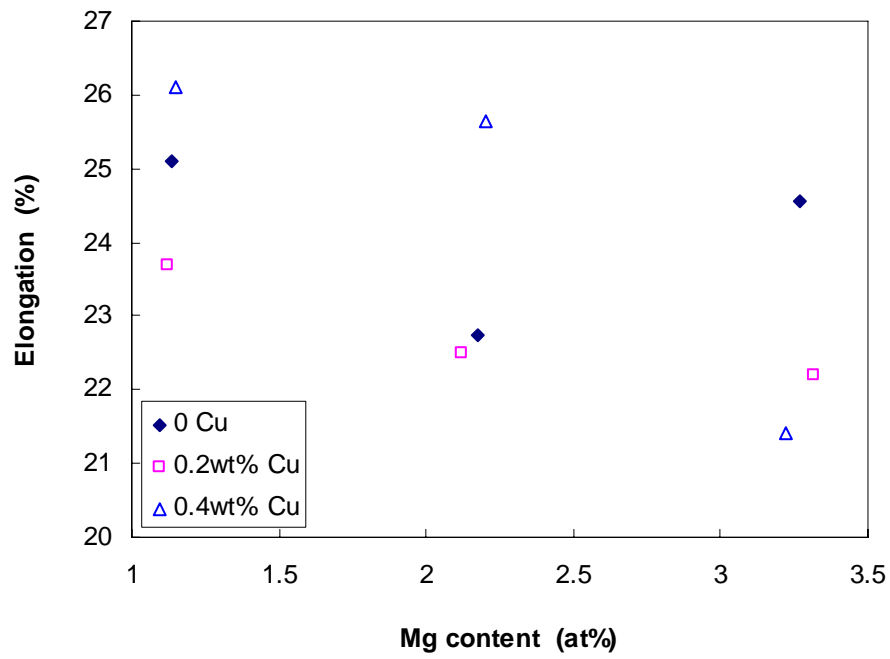$$\sigma_{rex} = \sigma_{gb} + M(\tau_o + \Delta\tau_{ss}) \qquad (2)$$

where $\Delta\sigma_{gb}$ is the strength increment due to the grain boundaries, M is a crystallographic orientation factor (often termed the Taylor factor) which is related to texture and the orientation of the specimen, τ_o is critical resolved shear stress of pure Al. The self-consistent modelling of the plastic deformation of FCC polycrystals gives M=2.6 [28].
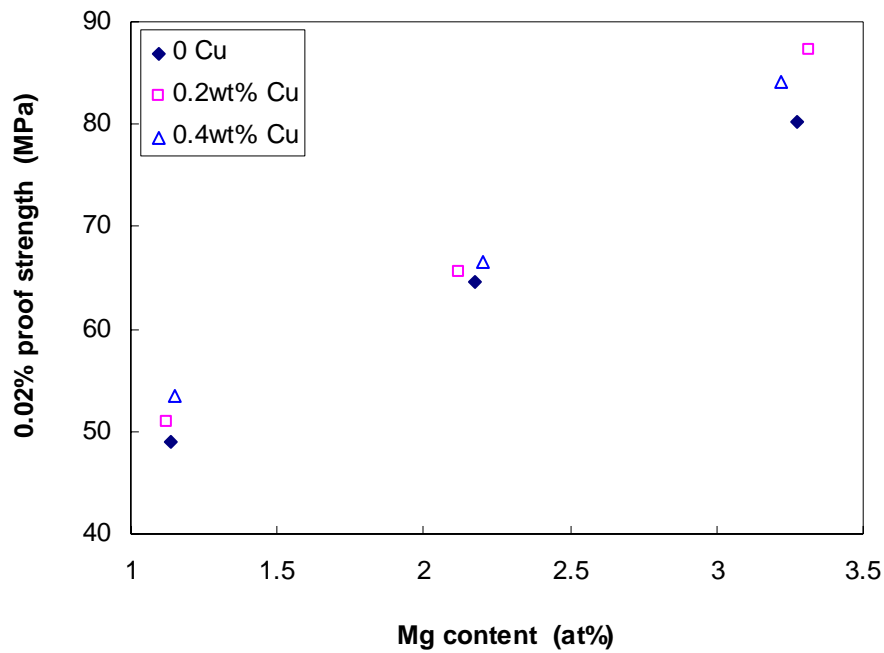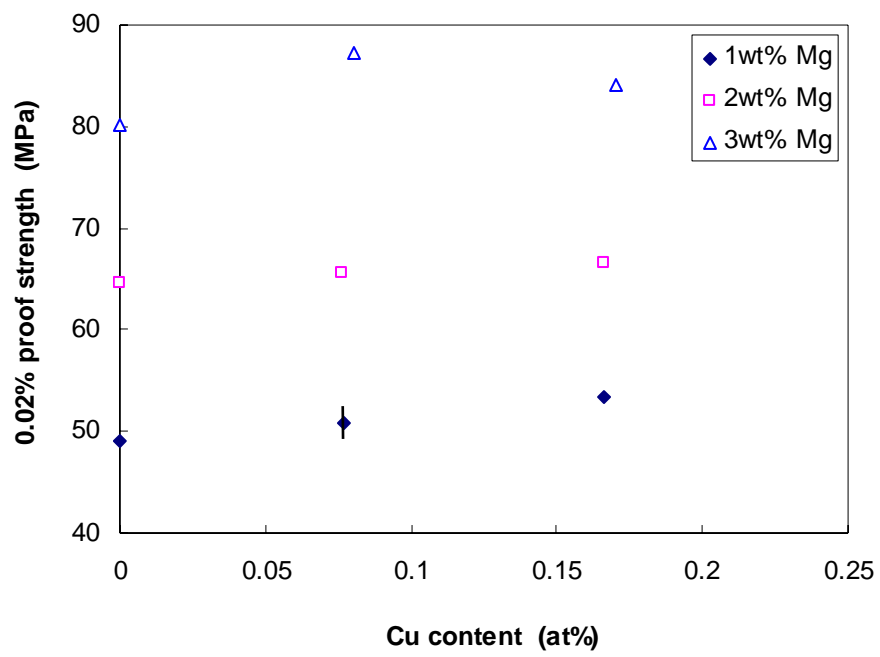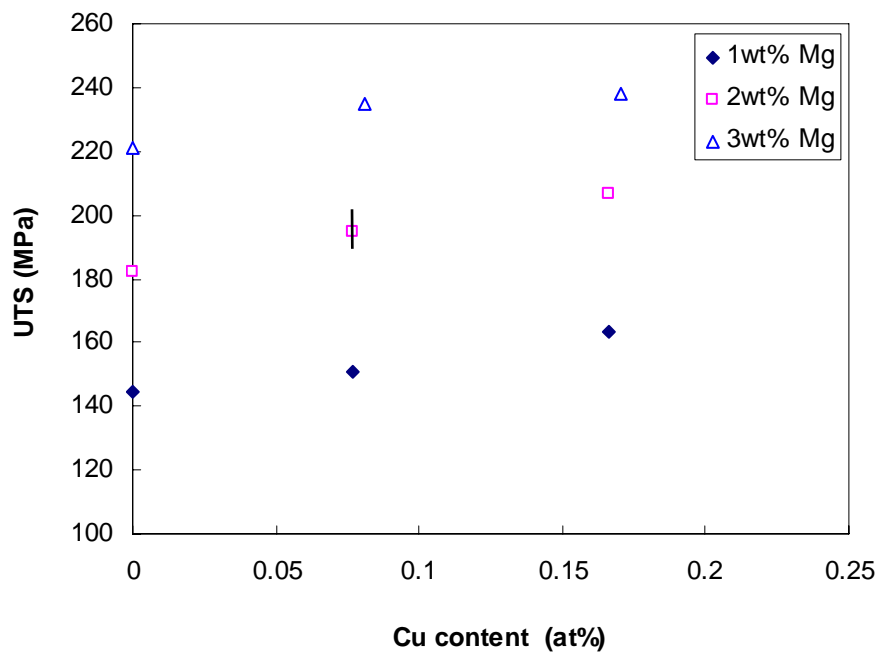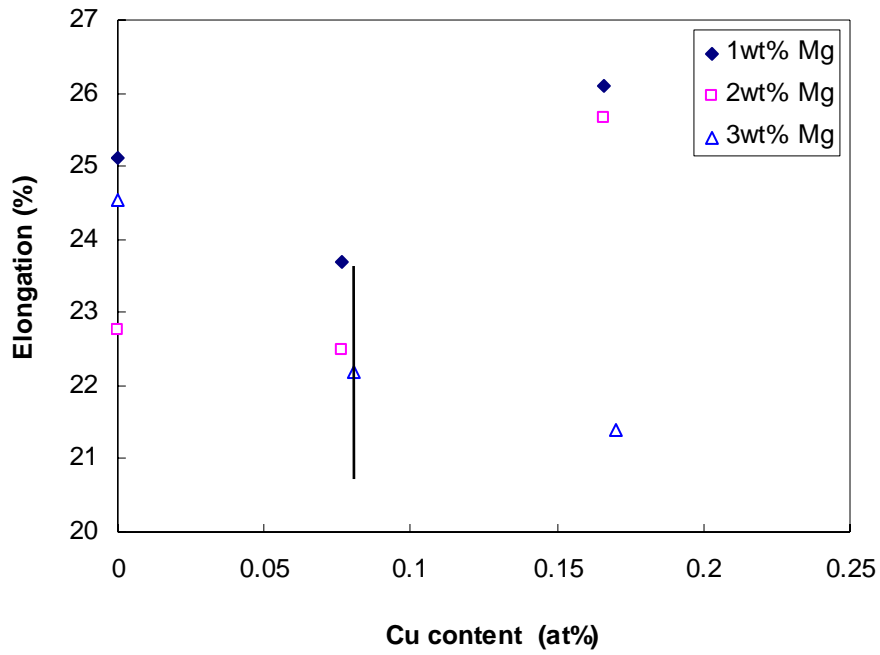

a.
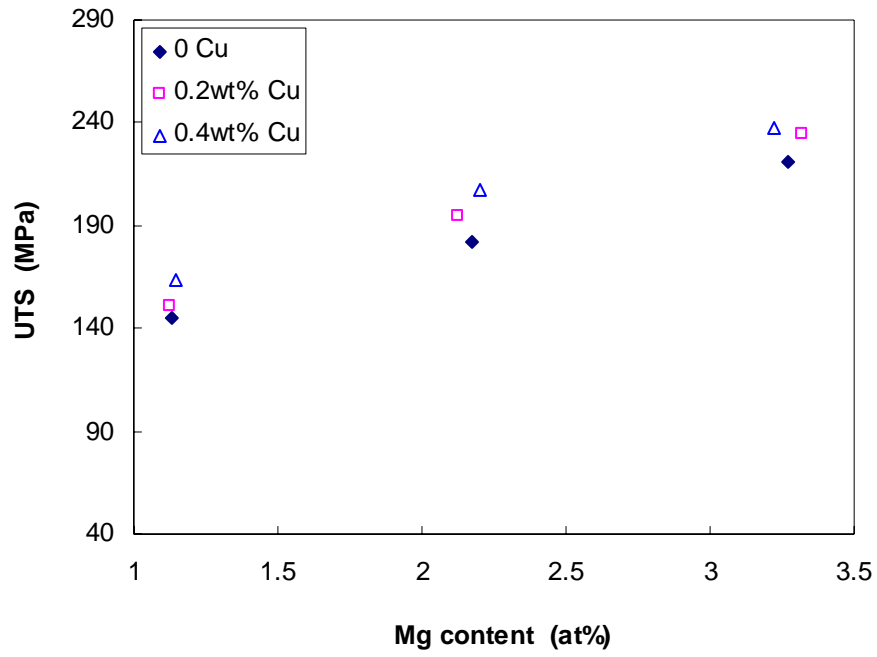
b.

c.

Fig. 3   Tensile test data vs. Mg contents for solution treated samples: a. 0.2% proof strength, b. UTS, c. elongation.

a.

b.

c.

Fig. 4   Tensile test data vs. Cu contents for solution treated samples: a. 0.2% proof strength, b. UTS, c. elongation. Bars on one point represent the average spread in measured values for each data point.
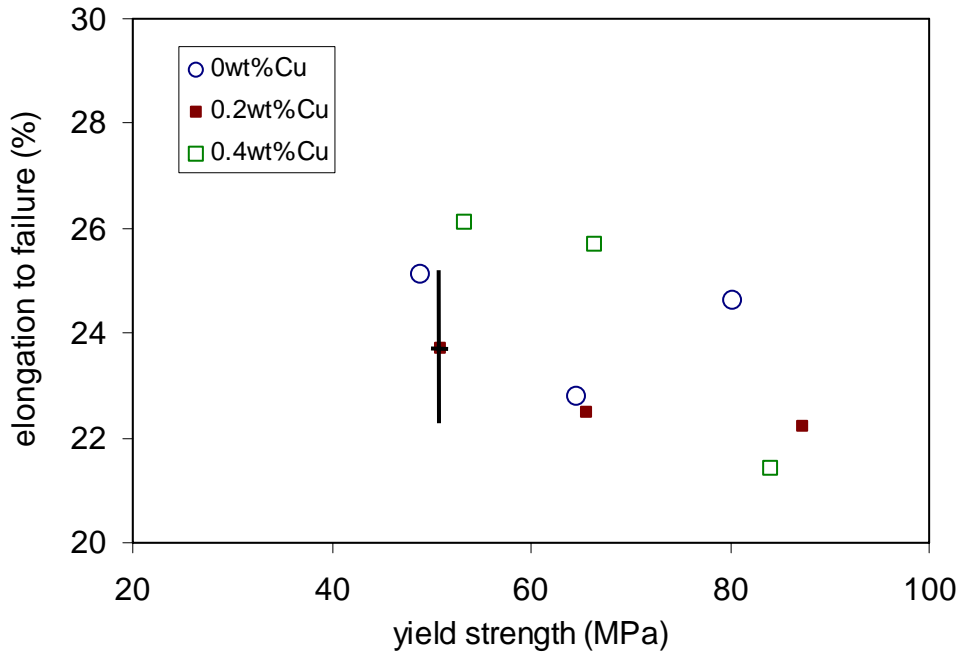

Fig. 5   Elongation to failure vs tensile yield strength for the 9 alloys in solution treated condition. Bars on one point represent the average spread in measured values for each data point.
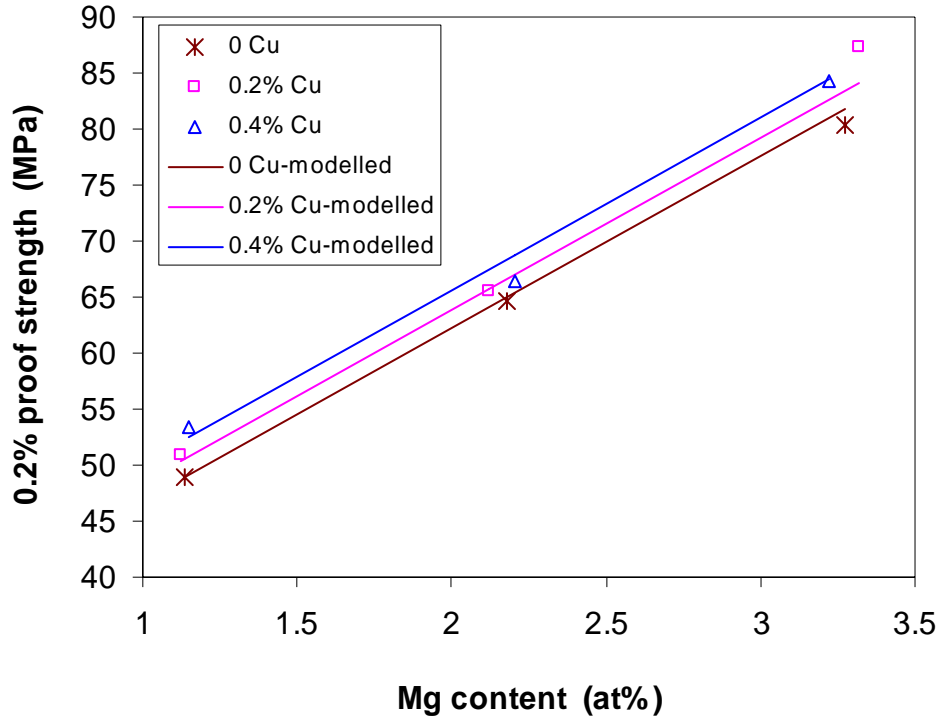
Fig. 6   Measured 0.2% proof strengths of solution treated alloys and their prediction.

The validity of Eq. 1 was tested by taking n_{SS} as 1, 2/3 or 1/2 respectively, and fitting the k parameters by the Least Square Method (LSM). Comparing the root mean squared error (RMSE) using different n_{SS} values, the lowest RMSE can be achieved when n_{SS} equals 1. This finding is consistent with other analyses of solid solution strengthening by Mg [27,29].

After these parameters were determined, the yield strength of the solution treated alloys can be modelled using equations 1-2, and the predicted results and experimental results are shown in Fig. 6. As shown in the figure, the predicted results reflect the experimental results very well with RMSE about 1.4 MPa. k_{Mg} determined this way is 590MPa (i.e. the CRSS increases by 5.9MPa per at%Mg), which compares to 540 MPa from data given in Ref. [30], and an analysis of literature data from the ASM Handbook [31] provides 570MPa [15].

3.3   Age hardening

The hardness during isothermal ageing at 170°C for samples after solutionising at 500°C and 550°C are presented in Fig. 7. As shown in the figure, all Cu-containing alloys and alloy A1 show age hardening. For Cu-free alloys A2 and A3, no substantial age hardening was observed after solutionising at 500°C, but after solutionising at 550°C these alloys do show age hardening (see Fig. 7b). In interpreting the hardening data we need to consider that for the present alloy compositions ternary Al-Cu-Mg precipitates, precipitates based on the Mg_2Si precipitation sequence and possibly quaternary Al-Mg-Si-Cu precipitates can cause strengthening (see e.g. [32]); whilst Mg contents are too low to allow precipitation of binary Al-Mg precipitates [33]. For instance, high-resolution transmission electron microscopy (HRTEM) studies of an Al-3Mg-0.4Cu-0.12Si (wt%) alloy during

artificial ageing at 180°C has shown the presence of coherent precipitates (crystal structure is orthorhombic Cmmm with lattice parameters a=1.2 nm, b=0.4 nm, c=0.4 nm), which on further ageing transform into S phase [34]. Our results in (Fig. 7) show that a wide range of alloy compositions with very low Si and Cu contents are age hardenable. Age hardening for Cu free alloys occurs presumably through formation of Mg_2Si type precipitates.
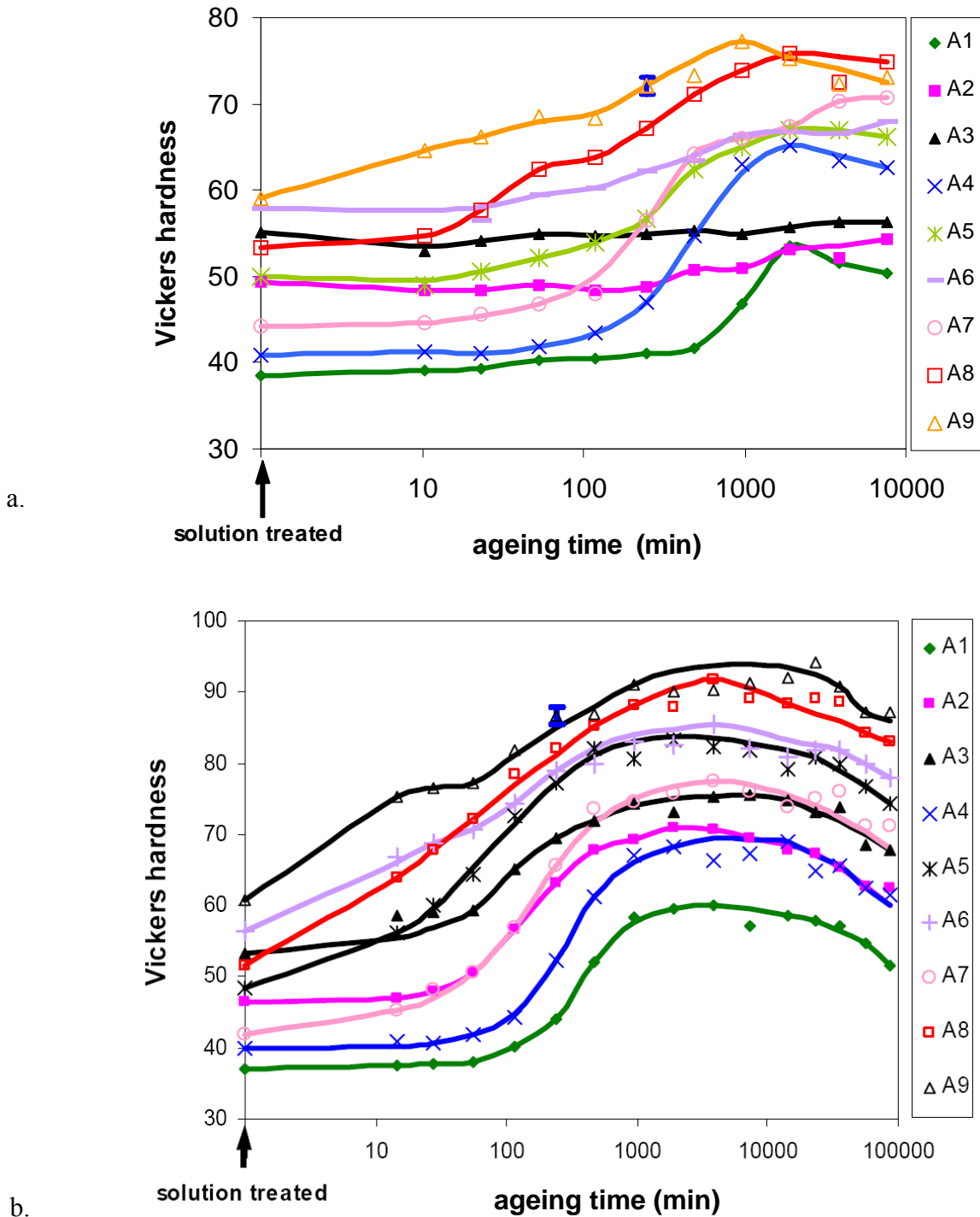

a.

b.

Fig. 7   Hardness during isothermal ageing at 170°C for solution treated samples solutionised 30 minutes at a) 500°, and b) 550°C. In each graph, one error bar is shown, which indicates the average of the standard deviations of all tests reported in that graph.
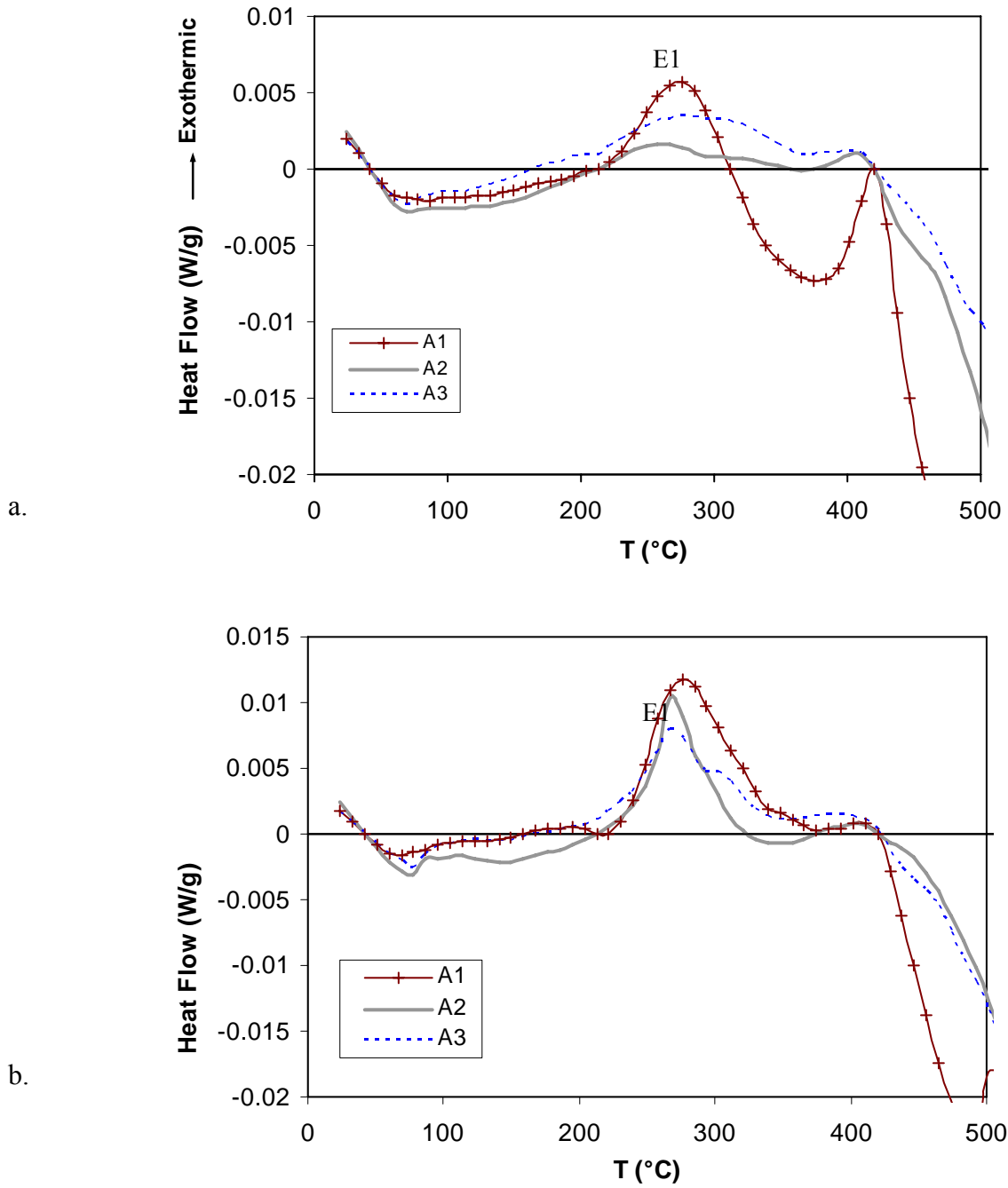
Fig.8 DSC data for Cu-free alloys solutionised 30 minutes at a) 500˚C, b) 550˚C

To further study the reactions responsible for age hardening, DSC experiments were performed on the alloys in solution treated condition. For all alloys exothermic reactions indicative of precipitation reactions [16] occur, see Fig.8 and Fig. 9. To compare the isothermal ageing treatments with non-isothermal treatments by DSC in this study, we can use the temperature compensated time for a single thermally activated reaction, which is defined as [16]:

$$\int \exp\left(-\frac{E_a}{RT}\right)dt = \exp\left(-\frac{E_a}{RT_{eq}}\right)t_{eq}$$
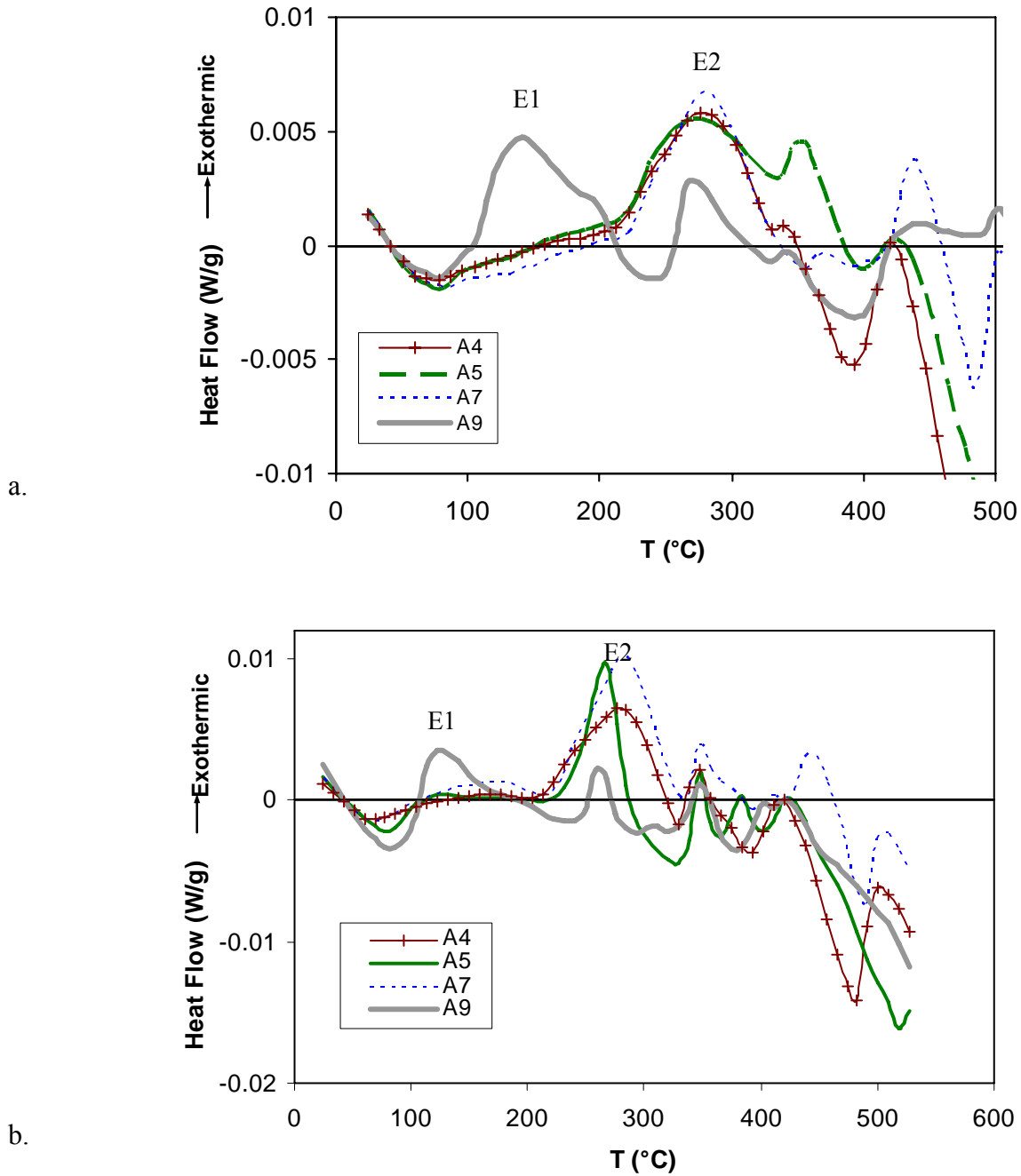
(3)

a.

b.

Fig. 9 DSC data for selected Cu-containing alloys solutionised 30 minutes at a) 500˚C, b) 550˚C

where E_a is the activation energy for the reaction (typically about 120 to 150 kJ/mole for precipitation reactions involving Si, Mg and Cu), R is the gas constant, T is a temperature reached during a non-isothermal treatment, T_{eq} and t_{eq} are an equivalent temperature and time in an isothermal heat treatment, respectively. The integral can be approximated in several ways [35,36]. From temperature-compensated time calculations it can be deduced that reactions related to age hardening, which complete within several days isothermal ageing at 170˚C, are related to reactions occurring during DSC heating up to 350˚C during DSC at a heating rate of 10˚C/min. Hence, an analysis of DSC data up to 350˚C may provide some interpretation of age hardening observed in the

alloys. For Cu-free alloys, as shown in Fig. 8, an exothermic effect E1 at temperatures around 200-300°C occurs in solution treated alloy A1, regardless of the solutionising temperature. However, for alloys A2 and A3, it only occurs when the alloys are solutionised at 550°C. This is consistent with the observation of age hardening of these three Cu-free alloys. The effect E1 in Fig. 8, which is likely to be due to the precipitation of Mg_2Si type precipitates, may be responsible for the age hardening observed during ageing for the Cu-free alloys. For Cu-containing alloys, the heat effects due to reactions become more complicated as shown in Fig. 9. An exothermic effect E2 at the temperatures around 200-300°C occurs in all solution treated Cu-containing alloys, regardless of the solutionising temperature. This is consistent with the observation of age hardening detected in all the Cu-containing alloys. This precipitation reaction is likely to be the main contributor to the age hardening of the alloys during isothermal ageing. For alloy A9 this effect is preceded by an exothermic effect at temperatures around 100-200°C, indicated as E1 (see Fig. 9). It occurs in alloy A9, regardless of the solutionising temperature. This effect is consistent with the observation of rapid hardening within 1h ageing (see Fig. 7b).

The SEM investigations (see section 3.1) showed that the cold rolled alloys with 1wt% Mg, which were solutionised at 500°C prior to cold rolling do not contain coarse Mg_2Si particles, whilst coarse Mg_2Si particles were observed in the alloys with higher Mg content. This suggests that for the alloy with 1wt% Mg (alloy A1), Mg_2Si particles can be dissolved at 500°C and thus Si becomes available for precipitation, and hence age hardening in this alloy is ascribed to the precipitation of Mg_2Si particles and their precursors (e.g. β" phase [37]). However, for alloys with Mg content in excess of 2wt% very limited Mg_2Si particles can be dissolved at 500°C and thus less Si is in solution and hence no substantial age hardening can be observed in alloys A2 and A3. However, the Mg_2Si particles can be dissolved at 550°C, hence these alloys show age hardening after solutionising at 550°C. This interpretation of Mg_2Si solubility for these alloys in the 500 to 550°C range is consistent with thermodynamic modelling predictions (see Table 2) and DSC analysis (see above). Thus the age hardening capability of these alloys is very sensitive to the combination of Mg content and solution treatment temperatures, which determine the amount of Si that is available for precipitation hardening.

All alloys show substantial age hardening after solutionising at 550°C (Fig. 7b). Compared with the results of ageing after solutionising at 500°C, the maximum hardness reached is higher and the hardening occurs at an increased rate. This enhanced age hardening rate may be due to an increased density of vacancies introduced at the higher solution temperature, which provides more nucleation sites for precipitation. It is interesting to note that after solutionising at 550°C, most Cu-containing alloys show rapid hardening within 1h ageing (Fig. 7b). But after solutionising at 500°C, only alloy A9 shows rapid hardening (Fig. 7a). This rapid hardening is though to be due to either Cu-Mg co-clusters [38,39] or S" phase [34] and is also consistent with the DSC analysis (see above).

We further compared the observed age hardening and the assumed existence of two precipitation sequences with predictions based on the theory of hardening through hampering of dislocation movement by obstacles. This theory predicts that in the absence of significant dislocation hardening the yield strength of a polycrystalline alloy is given by [40,41]:

$$\sigma_y \;=\; \Delta\sigma_{gb} + M\,\tau_{tot} \;=\; \Delta\sigma_{gb} + M\,[\,\tau_0 + \Delta\tau_{ss} + (\Delta\tau_{p,A}{}^2 + \Delta\tau_{p,B}{}^2)^{1/2}\,] \qquad (4)$$

where τ_{tot} is the total CRSS of the grains, $\Delta\tau_{p,A}$ and $\Delta\tau_{p,B}$ are the increments in CRSS of the grains due to precipitate type A and B, which in our alloys are the S phase and the Mg_2Si phase and its precursors. In our alloys the precipitates are approximately rod shaped, and for these particles it holds [42]:

$$\Delta\tau_{p,rod} = \frac{0.112\,\mu_{Al}\,b}{D_r}\ln\left(\frac{1.316\,D_r}{r_o}\right)\left(f^{1/2} + 0.94f + 2.44f^{3/2}\right) \qquad (5)$$

where μ_{Al} is the shear modulus of aluminium, f is the volume fraction of the rod-shaped precipitates, D is the diameter of the obstacle, b is the Burgers vector and r_o is the inner cut-off radius for calculation of the dislocation line tension, which is generally considered equal to the Burgers vector. For the very small volume fractions of precipitate encountered here we may approximate:

$$\Delta\tau_{p,rod} \cong \frac{0.112\,\mu_{Al}\,b}{D_r}\ln\left(\frac{1.316\,D_r}{r_o}\right)f^{1/2} \qquad (6)$$

In a further approximation we may consider that the diameter and aspect ratio of the precipitates at the peak of strength does not depend significantly on the alloy composition, and provided the two precipitates types reach their peak strengthening contribution at approximately the same ageing time, the precipitate strengthening contribution is proportional to the volume fractions as follows:

$$(\Delta\tau_{p,A}^2 + \Delta\tau_{p,B}^2)^{1/2} = (B_A f_A + B_B f_B)^{1/2} \qquad (7)$$

where B_A and B_B are constants depending on the diameter and aspect ratio of the precipitates at peak strength. This model for peak strength (Eq. 6 and 7) was fitted to the observed data on hardness increment caused by ageing (which ranges from 0 to 39HV) using the assumption that hardness is proportional to yield strength. To this end we assume that the precipitate stoichiometry is independent of alloy composition and fit B_A and B_B to the data. A good correlation (standard deviation 3HV, which is 8% of the observed range) of modelled and measured peak hardness (from Fig. 7a) is obtained. (It should be noted that when alloy A5, which appears to have a somewhat high peak hardness, is omitted the standard deviation improves to 2HV.) This good correlation shows that the observed peak hardness values are indeed consistent with the present interpretation of two precipitates being responsible for peak hardness. Higher than predicted hardening increments are observed for alloys A5, A8 and A7 (in order of highest deviations). These alloys are close together in terms of Mg:Cu:Si ratios which might hint at further details relevant to precipitation hardening beyond the simplified approximations considered here. It might for instance hint at the occurrence of quaternary precipitates.

It should be noted that Vooijs et al. [43] have studied precipitation in solution treated (at 610°C) and solution treated and subsequently cold rolled Al-0.9Mn-0.97Mg-0.18Cu-0.0.46Fe-0.29Si and Al-1.04Mn-1.36Mg-0.30Cu-0.31Fe-0.17Si alloys (in wt%) by using thermoelectric power and resistivity measurements. In agreement with our analysis they concluded that S precipitates (Al_2CuMg) form at ageing temperatures below 225°C but they stated that only a very small amount of Mg_2Si forms. Our analysis indicates that for the very similar alloy A4, Si containing precipitates are significant, with the strengthening contributions from the two types of precipitates of similar

order of magnitude. One explanation may be the larger Mn content of Vooijs et al.'s alloy which may lead to increased amounts of the Si containing $Al_{12}(Fe,Mn)_3Si$ remaining undissolved during the solution treatment. We would also note here that the analysis in [43] using a combination of thermoelectric power and resistivity measurements might produce some inaccuracy with regards to the ratio of S and Mg_2Si precipitates due to a non stoichiometric composition of the Mg_2Si precipitates and electron scattering effects by very small precipitates.

4   Conclusions

Nine Al-(1-3)Mg-(0-0.4)Cu-0.15Si-0.25Mn (in wt%) alloys with potential and existing applications in both packaging and automotive industries have been investigated. Tensile testing at room temperature of solution treated samples showed that solution strengthening in good approximation increases linearly with Mg content. In solution treated condition, the alloys have elongation to failure between 22 and 26%; Cu additions have a very limited influence on elongation. Hardness testing and DSC analysis of solution treated and aged samples indicate that Mg_2Si phase precipitates contribute to age hardening of Cu-free alloys, whilst both Mg_2Si phase and S (Al_2CuMg) phases contribute to that of Cu-containing alloys. The age hardening capability is critically influenced by solution treatment temperature: increasing the solution treatment temperature from 500 to 550⁰C results in a marked increase in rate of hardening for Cu containing alloys and solution treatment at about 550⁰C or higher is needed to allow Mg_2Si phase precipitation during ageing in Cu-free alloys with Mg content of about 2% or higher.

References
[1]   J. Courbon, Mater. Sci. Forum, 331-337 (2000) 17.
[2]   J. Courbon, Scr. Mater. 48 (2003) 1519-1524.
[3]   K. Koyama, S. Urayoshi, T. Tanaka, Furukawa Review 18 (1999) 97.
[4]   G.J. Marshall, Mater. Sci. Forum 217-222 (1996) 19.
[5]   G.B. Burger, A.K. Gupta, P.W. Jeffrey, D.J . Lloyd, Mater. Charact. 35 (1995) 23.
[6]   P. Ratchev, B. Verlinden, P. van Houtte, P. de Smet, Mater. Sci. Eng. A 222 (1997) 189.
[7]   Herdawandi Halim, D.S. Wilkinson, M. Niewczas, Acta Mater. 55 (2007) 4151-4160.
[8]   S.A. Court, K.M. Gatenby, D.J. Lloyd, Mater. Sci. Eng. A 319 (2001) 443 -447.
[9]   Y. Birol, Mater. Sci. Techn. 22 (2006) 987-994.
[10]   P. Ratchev, B. Verlinden, P. de Smet, P. van Houtte, Acta Metall. Mater. 46 (1998) 3523.
[11]   D.T.L. Alexander, A.L. Greer, Acta Mater. 50 (2002) 2571 -2583.
[12]   R.K. Bolingbroke, G.J. Marshall, R.A. Ricks, R.A., the 3rd International conference on Aluminium alloys, L. Arnberg, O. Lohne, E. Nes, N. Ryum (Eds), 1992, Trondheim, Norway, p. 285
[13]   B. Verlinden, A.-M. Zahra, Mater. Sci. Forum 426-432 (2003) 423.
[14]   M.J. Starink, A. Dion, Thermochim. Acta 417 (2004) 5-11.
[15]   S.C. Wang, Z. Zhu, M.J. Starink, J. Microscopy 217 (2005) 174–178.
[16]   M.J. Starink, Int. Mater. Rev. 49 (2004) 191-226.
[17]   M. Dehmas, P. Weisbecker, G. Geandier, P. Archambault, E. Aeby-Gautier, J. Alloys Compounds 400 (2005) 116-124.

[18] N.A. Lange, G.M. Forker, Lange's Handbook of Chemistry. (10th edition). McGraw-Hill Book Company: New York (1967).

[19] C. Blanc, Y. Roques, G. Mankowski, Corrosion Sci. 40 (1998) 1019.

[20] M.C. Sneed, R.C. Brasted, The elements and compounds of group IVA (Vol.7). Comprehensive inorganic chemistry. New York: D. Van Nostrand Company, INC. (1958).

[21] J. Friedel, Dislocations. London: Pergamon Press Ltd. (1964).

[22] A.J.E. Foreman, M.J. Makin, Phil. Mag. 14 (1966) 911-924.

[23] F. Nabarro, Theory of crystal dislocations. Oxford: University Press (1967).

[24] L.A. Gypen, A. Deruyttere, J. Mater. Sci. 12 (1977) 1028.

[25] P. Gomiero, Y. Brechet, F. Louchet, A. Tourabi, B. Wack, Acta Metall. Mater. 40 (1992) 857.

[26] P. Haasen: in Physical Metallurgy, 4th ed., R.W. Cahn and P. Haasen, eds., Elsevier Science BV, 1996, pp. 2009-68.

[27] O. Nijs, E. Sjolander, B. Holmedal, H.E. Ekstrom, E. Nes, Metall Mater Trans 37A (2006) 1999 - 2006.

[28] B. Clausen, T. Lorentzen, T. Leffers, Acta Mater. 46 (1998) 3087.

[29] J. Yan, PhD thesis, University of Southampton, 2006.

[30] D.J. Lloyd, S.A. Court, Mater. Sci. Technol. 19 (2003) 1349.

[31] Davis, J.R., ASM Specialty Handbook: Aluminium and Aluminium Alloys. ASM International (1993).

[32] D.J. Chakrabarti, D.E. Laughlin, Prog. Mater. Sci. 49 (2002) 389-410

[33] M.J. Starink, A.-M. Zahra, Phil. Mag. A 76 (1997) 701-714.

[34] L. Kovarik, P. I. Gouma, C. Kisielowski, S. A. Court, M. J. Mills, Acta Mater. 52 (2004) 2509-2520.

[35] M.J. Starink, Thermochim Acta 404 (2003) 163.

[36] M.J. Starink, J. Mater. Sci. 42 (2007) 483-489.

[37] M.A. van Huis, J.H. Chen, M.H.F. Sluiter, H.W. Zandbergen, Acta Mater. 55 (2007) 2183-2199.

[38] M.J. Starink, N. Gao, L. Davin, J. Yan, A. Cerezo, Phil. Mag. 85 (2005) 1395-1418.

[39] M.J. Starink, N. Gao, J.L. Yan, Mater. Sci. Eng. A 387-389 (2004) 222-226.

[40] M.J. Starink, A. Deschamps, S.C. Wang, Scr. Mater, 2007, in press

[41] M.J. Starink, S.C. Wang, Acta Mater. 51 (2003) 5131-5150

[42] I.N. Khan, M.J. Starink, J.L. Yan, Mater Sci Eng A, 2007, in press

[43] S. Vooijs, B. Davenport, I. Todd, S. van der Zwaag, Philosph Mag A 81 (2001) 2059